Fabrication of ITO microelectrodes and electrode arrays using low-cost CO_2 laser plotter

Karthika Kappalakandy Valapil,[a] Marcin Szymon Filipiak,[a] Weronika Rekiel,[a] Elżbieta Jarosińska,[a] Martin Jönsson-Niedziólka[a], Emilia Witkowska Nery[a]*

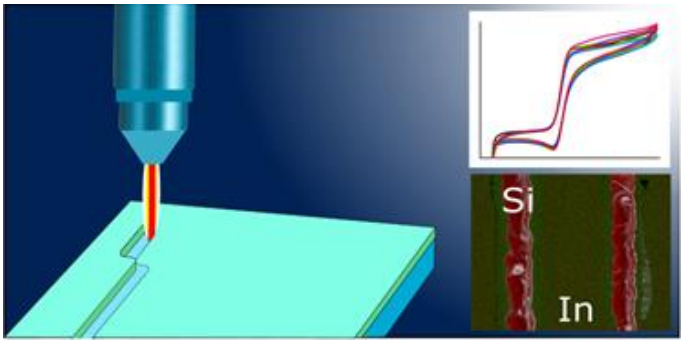

Excellent electronic and optical properties make indium tin oxide (ITO) an attractive electrode substrate. Despite the commercial availability of high-quality ITO and some low-cost methods for direct deposition being in use by now, the definition of patterns is still a concern. Putting its popularity and extensive usage aside, the manufacturing of ITO electrodes so far lacks a rapid, highly reproducible, flexible, cost-effective, easy patterning process that could surpass difficult, time-consuming techniques such as lithography. A cost-effective method based on CO_2 laser irradiation for preparing ITO microelectrodes and electrode arrays is presented herein. Electrodes of different sizes and shapes were examined to identify the performance of the proposed methods. Direct ablation of the ITO layer was optimized for rectangular electrodes of 25, 50, and 100 μm width, while laser cutting of scotch tape stencils and subsequent wet etching were used to create circular electrodes with a diameter of 1.75mm. Together, both methods form a complete toolbox, which allows for low-cost and fast fabrication of ITO electrodes for wide variety of applications. A multielectrode array system consisting 8 of these circular electrodes was fashioned, fabricated, assembled, and tested. The ITO electrodes were characterized electrochemically and as an example application they were used for monitoring anchoring behavior of HeLa and HepG2 cell cultures through cell-based electrochemical impedance technique.

Introduction

Indium tin oxide (ITO) is transparent and colorless as a thin film and yellowish to grey in the form of bulk material. It is a solid solution of indium oxide (In_2O_3) and tin oxide (SnO_2) typically in a weight ratio of 90:10[1]. Conventionally, it is being employed as an electrode substrate due to its excellent electronic and optical properties such as low electrochemical background response, wide working potential window[2], low resistivity, high visible transmittance, high infrared reflectivity, and ultraviolet absorption[1,3]. Qualities like good surface area activity, machinability, high chemical stability, inertness, and commercial availability make it desirable for scientific purposes. ITO is widely applied in optoelectronics[4], mostly in light-emitting diodes[5], liquid crystal displays[6], solar cells[7], transistors[8], and gas sensors[9], but is also commonly used in electrochemistry for electroanalytic devices[10], sensing[11] and biosensing[12].

With high quality ITO being readily available commercially and methods for direct deposition already in use[13,14], the definition of patterns is still another potential bottleneck. Despite being popular and widely used, the manufacturing of ITO electrodes still lacks a rapid, flexible, cost effective and precise fabrication method that could supplement expensive and time consuming lithography most often used for defining patterns. The use of lasers for the fabrication of ITO electrodes marked a promising development towards achieving highly reproducible, flexible, fast, and easy patterning. Laser Digital Patterning (LDP)[15] and Pulsed Laser Deposition (PLD)[16] processes for fabrication of ITO electrodes are examples of these kind. A nanosecond Nd: YAG infrared laser for indirect laser ablation to pattern ITO on its glass substrate was reported[17]. Another interesting example is the pattern formation on ITO films coated on borosilicate glass by scanning a linearly polarized nanosecond pulsed laser beam, making use of a self-organization phenomenon named laser-induced periodic surface structures (LIPSS)[18]. Apart from these examples, there are other reports on laser patterning of ITO using other lasers, such as an UV-excimer laser and femtosecond-pulsed laser[19], but none of these gives the advantage of being widely available and preferably affordable means of fabrication of microelectrodes.

Currently, CO_2 lasers, emitting infrared radiation at a wavelength of 10.6 μm, are the highest power continuous wave lasers available. With their high efficiency they are commonly used in laser cutting, welding, drilling and surface treatment[20]. But they are also used in applications for processing of components for microfluidic systems. A novel laser through- cutting and pattern transfer process was introduced for rapidly prototyping polydimethylsiloxane (PDMS) microfluidic structures without a replication template using a CO_2 laser that significantly decreases the time and amount of equipment and consumables needed for microchannel processing[21]. Using laser cutting for quickly transferring a pattern drawn in a computer aided design (CAD) program to a plastic film or PDMS slab for microfluidics, sometimes known as xurography, has risen in popularity as CO_2 laser cutters have become more affordable and easier to use[22]. Based on this technology a microfluidic sensor which was used to evaluate the biomass of the MRC-5 fibroblast cells grown in the microfluidic bioreactor was recently presented[23]. In addition to traditional PDMS channels, CO_2 lasers have also been used for patterning paper-based microfluidic systems and modifying the surface properties of the paper[24,25]. CO_2 laser processing has also been used to directly make electrodes by carbonisation of polymers to create laser-induced graphene (LIG) materials, either freestanding or on a backing material, like ITO and this offers a possible advancement towards reducing the high cost of exploiting the laser technology for sensing applications[26,27].

In this article, we used computer aided design in Autocad, to directly imprint a desired electrode pattern on ITO coated glass surfaces with the help of a CO_2-laser. The process was optimized to obtain electrodes with widths as small as 25 μm. The electrodes thus obtained were characterised using electrochemical methods and optical and scanning electron microscopes were used to identify the geometric parameters of the electrodes. A supplementary method was used for creation of larger area electrodes where the high resolution of direct laser cutting was not necessary, in which a stencil was prepared using the laser and the undesired ITO, outside the electrodes was removed by wet-etching. This method is much more efficient than direct cutting of big areas using the laser, but suffers lower resolution. Both methods together form a complete toolbox, which allows for low-cost and fast fabrication of ITO electrodes for wide variety of applications.
In the end the fabricated electrodes are applied for analysis of cell cultures using impedance spectroscopy. Cell-based impedance studies measure changes in electrical impedance relative to a voltage or current applied to the electrodes covered with cell layer. It uses the principles of electrochemical impedance spectroscopy (EIS) and enables a platform for the recognition of several characteristics of cell cultures corresponding to the metabolism, adhesion, viability, motility and proliferation[28]. We employed a well fashioned device with a planar array of 8 circular ITO electrodes to monitor the state of HepG2 and HeLa cell cultures, during their seeding, attachment to the electrode surface and trypsin induced detachment from the substrate.

Methods

Chemicals

The chemicals 1,1'-ferrocenedimethanol (98%, Acros Organics), KNO_3 (99%, POCh), $CuSO_4x5H_2O$ (pure p.a., Chempur), acetic acid (99.5% pure p.a., Chempur), and sodium acetate trihydrate (≥ 99.0%, Sigma-Aldrich) were used as received. Water was filtered and deionized with an ELIX system (Millipore).

Direct laser ablation of ITO patterns

A clean 25 x 50 x 1.1 mm ITO covered (~130 nm, R_s = 5 - 15 Ω/sq) glass plates obtained from Delta Technologies (Loveland, CO, USA) were patterned directly (ablated) with a desktop CO_2 laser engraving machine – C180II purchased from GCC (New Taipei City, Taiwan) using a CAD design with the following parameters: speed 2.0, power 1% and PPI 1500 (Fig.1). The laser locally heats up the ITO layer on glass to the point it cracks and detaches from the glass plate. Finally, the ITO plates were sonicated in acetone, isopropanol, and distilled water for 15 minutes each. Each test plate consisted of 8 electrodes. Copper tape was used improving the electrical connections to the potentiostat and Kapton tape for masking the connections so that only the electrodes were exposed.

Laser ablation of scotch tape stencils and chemical etching of the ITO patterns

Clean 25 x 25 x 1.1 mm ITO covered (~260 nm, R_s = 4 - 5 Ω/sq) glass plates obtained from Biotain Crystal (Fujian, China) were covered with Scotch Magic Tape® purchased from 3M (Saint Paul, MN, USA). The same laser engraver was used to cut the tape using a CAD design with the following parameters: speed 3.0, power 1%, PPI 1500. After the patterning, the tape in undesired areas is removed and the plates are submerged in etchant solution (50 g $FeCl_3$ x $6H_2O$ + 80 mL distilled water + 20 mL of conc. 36% HCl) for 2.5 min at 60°C. The ITO plates were then sonicated for 15 minutes each in acetone, isopropanol, and distilled water to obtain 8 clean electrodes on every plate (Fig.2).

Electrochemical Measurements.

All the electrochemical measurements unless stated otherwise were performed with PalmSens4 potentiostat galvanostat, with an Electrochemical Impedance Spectroscopy (EIS) module, which is controlled with PSTrace software (version 5.8.1704). The three-electrode electrochemical cell consisted of a platinum wire counter electrode, Ag/AgCl (1M KCl) reference electrode, and ITO working electrodes.
The performances of the fabricated electrodes were first studied using cyclic voltammetry (CV) technique with 1,1'-ferrocenedimethanol (FcDM) as the redox probe in potassium nitrate. Parameters for CV were as follows: scan rate 0.01V/s, step potential 0.005 V. Electrodes were cleaned first with ethanol, then with water, and dried before the measurements. Apart from this 3 cycles of a step chronoamperometry was performed to analyse the real electrochemical active area using chronocoulometry, during which the initial potential 0.0 V was held for 10.0 seconds after which the potential stepped to 0.65 V for a time interval of 10.0 seconds.

SEM Imaging

Scanning Electron Microscope (SEM) micrographs of the electrodes were captured using a FEI Nova Nano – SEM 450 with an EDAX Octane Elect Plus EDS system. EDS mapping were performed of the elements Si and In. The width of the electrodes was measured from the SEM images (see SI Fig 3) using ImageJ.

Optical microscopy

Qualitative analysis of the electrode structures was carried out using a Nikon ECLIPSE LV150 optical microscope. The width of the electrodes was measured and compared to the nominal width from the laser cutter.

Routine cell culture

HeLa and HepG2 cell lines came from the American Type Culture Collection (ATCC, Manassas, USA). Both cell lines were cultured as a standard monolayer in the complete growth medium, supplemented with fetal bovine serum 10% v/v (FBS, Gibco), L-glutamine 1% v/v (Sigma-Aldrich), and the antibiotics: streptomycin [10 000 U ml^{-1}] and penicillin [10 mg ml^{-1}] 1% v/v (Sigma-Aldrich). Cultures were performed under standard conditions (37°C, 5% CO_2). Both cell lines were cultured in Dulbecco's Modified Eagle's Medium

(DMEM) with low glucose content (1g/L) (Institute of Immunology and Experimental Technology, Wroclaw, Poland). Using regular passages, cells were maintained in a logarithmic growth phase. To detach cells from the surface, 0.25% Trypsin–EDTA solution (Sigma-Aldrich) was used.

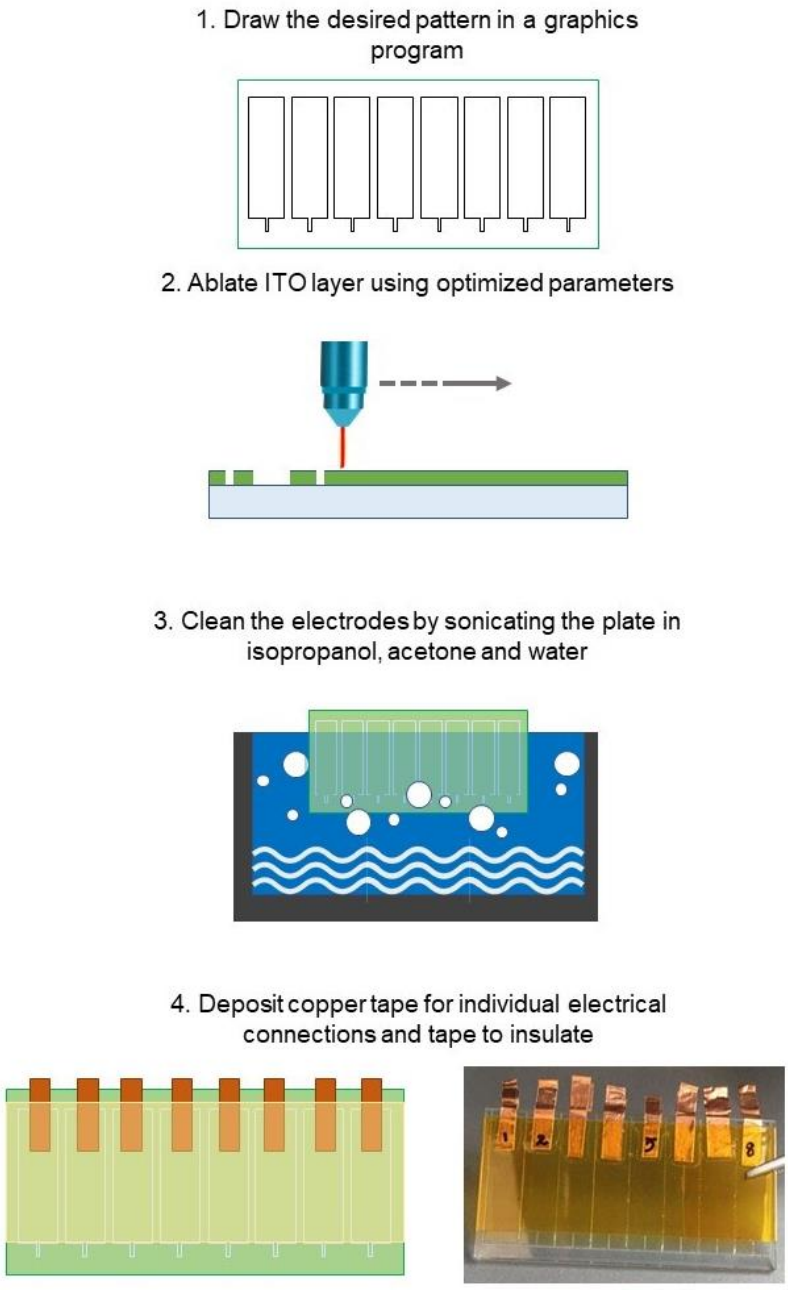

Fig. 1 Step-by-step fabrication procedure of the directly ablated patterns.

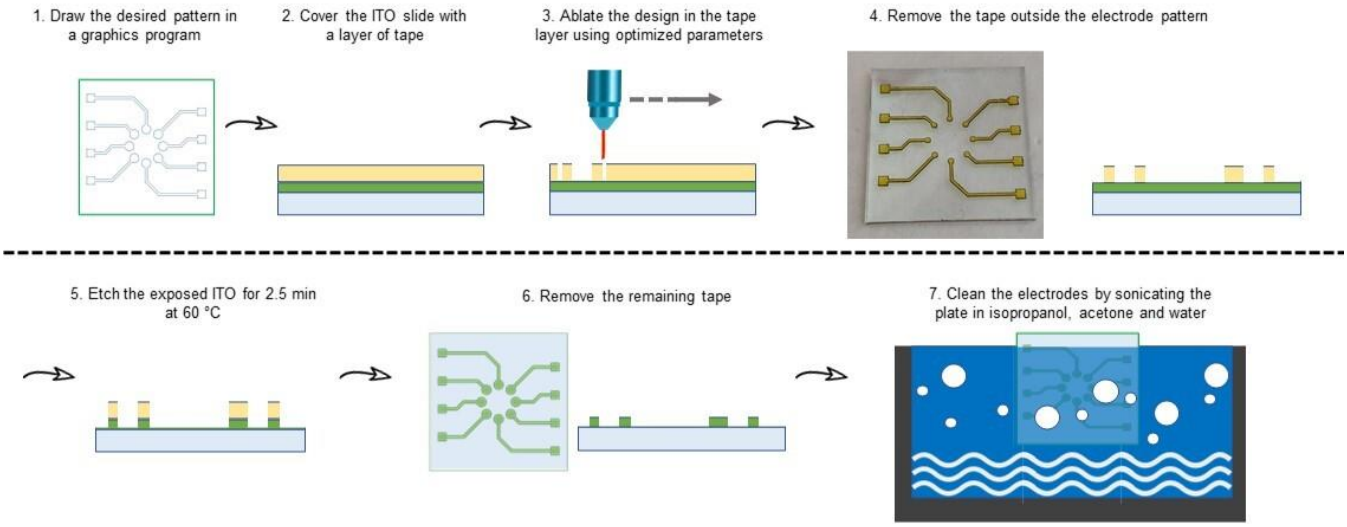

Fig. 2 Step-by-step procedure of the electrode fabrication using laser-ablated stencils.

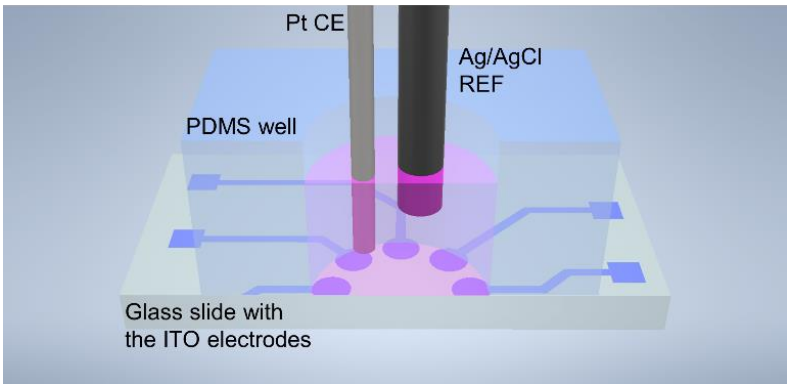

Fig. 3 Schematic representation of the measurement setup used for impedance spectroscopy of cell culture.

Cell culture monitoring using Impedance spectroscopy

All the impedance spectroscopy experiments unless stated otherwise were performed with PalmSens4 potentiostat galvanostat, with an Electrochemical Impedance Spectroscopy (EIS) module, which is controlled with PSTrace software (version 5.8.1704). The three-electrode electrochemical cell consisted of a platinum wire counter electrode, Ag/AgCl (1M KCl) reference electrode, and ITO working electrodes.

Prior to measurements, the cells were placed at a specific density on ITO electrode plate for cell culture monitoring utilizing impedance-based analysis. Experiments were performed in a closed, heat controlled chamber at 37°C. A complete Dulbecco's Modified Eagle's Medium (DMEM), supplemented with fetal bovine serum 10% v//v (FBS, Gibco), L-glutamine 1% v/v (Sigma-Aldrich), and the antibiotics: streptomycin [10 000 U ml^{-1}] and penicillin [10 mg ml^{-1}] 1% v/v (Sigma-Aldrich), with low glucose content (1g/L) (Institute of Immunology and Experimental Technology, Wroclaw, Poland), suitable for HeLa and HepG2 cell lines was used.

The cells have an adhering nature, once they attach to the working electrode surface they tend to impede the current flow between the electrodes. This refers to the current passing through available cell-substrate space as well as through intercellular passages. When the cells approach confluence on the electrode, the impedance fluctuates visibly and changes at an accelerated rate[29].

Impedance measurements were conducted over a range of 37 frequencies on HeLa cells since multiple research have recorded readings at various frequencies[29,30]. In our case, the frequency range were set between the limits 10Hz and 40kHz. For frequencies between 100 and 10kHz, the data from these measurements showed a noticeable increase in the impedance value that corresponds to growth of insulating character of the electrodes due to the cells getting attached on their surface. At higher frequencies a less pronounced change is observed, with a small increase in the impedance values that can be correlated to the increase of resistance at the working electrode-electrolyte interface. To understand the frequency that suits our measurements the best, we limited our studies to three frequencies (100 Hz, 2 kHz, and 10 kHz) between the range of 100 to 10kHz. Highest phase angle shift and rise of the impedance values of the cells

with respect to the blank (in our case DMEM) was observed at 100 Hz, thus the operating frequency was optimized as 100 Hz and experiments were conducted at 0.2V against OCP.
The majority of these measurements were brief, lasting about two hours. When the potentiostatic experiments first started, the electrode well was simply filled with 150μL of DMEM, and impedance was recorded for 30 minutes. Then, the medium in the well was spiked with 150μL of cells with a density of 1.33 x 10^6 cells/mL to give a final concentration of 6.65 x 10^5 cells/mL to observe their adhesion to the electrodes and how the later's surface is affected. Finally, at the 90th minute, 150μL of trypsin was introduced, and the system was monitored for 30 minutes more, before the impedance tests were terminated.

Results

Microscopic analysis

Initially, the electrodes were inspected using optical microscopy. In low magnification the electrodes look very nice and regular, but at higher magnification cracks and irregularities are seen, especially for the smaller electrodes (Fig 4). Measuring the width of the electrodes show that the narrower electrodes are significantly wider (39±3.5 μm) than the nominal width (25 μm).
To make sure that there was no electrical connection between the individual electrodes and other parts of the ITO-plate, a negative potential of -1.5V (vs. Ag/AgCl) was applied to ITO working electrode for a duration of 60 seconds. This results in the reduction of ITO layer. A significant change in the appearance of electrodes was observed, indicating disintegration of the electroactive area to metallic indium and tin as the electrode lost its transparency and appeared darker[31]. The reduced area is confined to the electrode and shows that there are no electrical connections with other parts of ITO.
The electrodes were also studied using SEM and EDX. The width of the electrodes were measured for SEM images at several positions along the length of each electrode on a plate. In the figure SI 3 we see that the widths of the electrodes, as measured by SEM, is larger than the nominal widths. In the EDX measurements we concentrated on the elements indium and silicon. When the electrodes are cut EDX data clearly show that the ITO is removed along the cut. Fig 4d shows cross sections of the indium signal for electrodes 25, 50 and 100 μm.

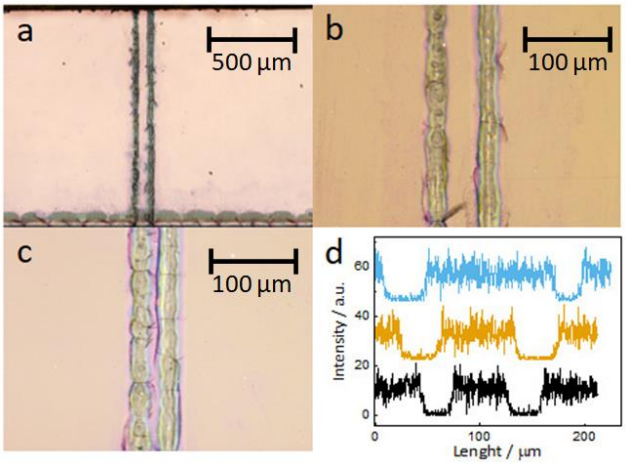

Fig.4 Microscopic image of an electrode with nominal width 100 μm a) 2.5X magnification, b) 5X magnification, c) microscopic image of an electrode with nominal width 25 μm at 5X magnification, d) EDX spectra of the ITO electrodes depicting intensity of indium on them.

Electrochemistry

The ITO electrodes prepared using CO_2 laser irradiation were primarily characterized using cyclic voltammetry (CV) and chronoamperometry (CA). Diffusion- controlled CVs with reproducible signals were observed for electrodes of all the sizes within the same plate. The plate-to-plate reproducibility of signals was highly satisfactory too. The figure 5 shows the reproducible cyclic voltammograms of electrodes of different sizes, where each set comes from a single plate.

Reproducibility

To illustrate the variations in the current response of the electrodes we performed cyclic voltammetry with electrodes from several batches in the redox probe FcDM. Current values of the working electrodes at the potential of 0.29V were plotted against their sizes. The 100μm wide electrodes had the most reproducible structures, these electrodes, therefore exhibited most uniform current ranges among the three sizes, within each plate. A lower reproducibility between different batches was observed for 100μm electrodes (Fig.6), which can be the result of a manual error occurred during the pasting of the Kapton tapes making length of the electrodes 10 to 15% shorter or longer. The smaller sizes, 50 and 25 μm, exhibited higher intraplate variability, this can be easily identified form the figure 5. The current value does not scale with size for 50 and 100μm wide electrodes (Fig.6), which might be caused by different activity of ITO at the edges of the electrodes caused by the laser ablation. The electrodes are of rectangular shape with 2.5 mm length and three different widths. These structures can also be tailored to different dimensions, for example shorter length resulting in microelectrodes of smaller area.

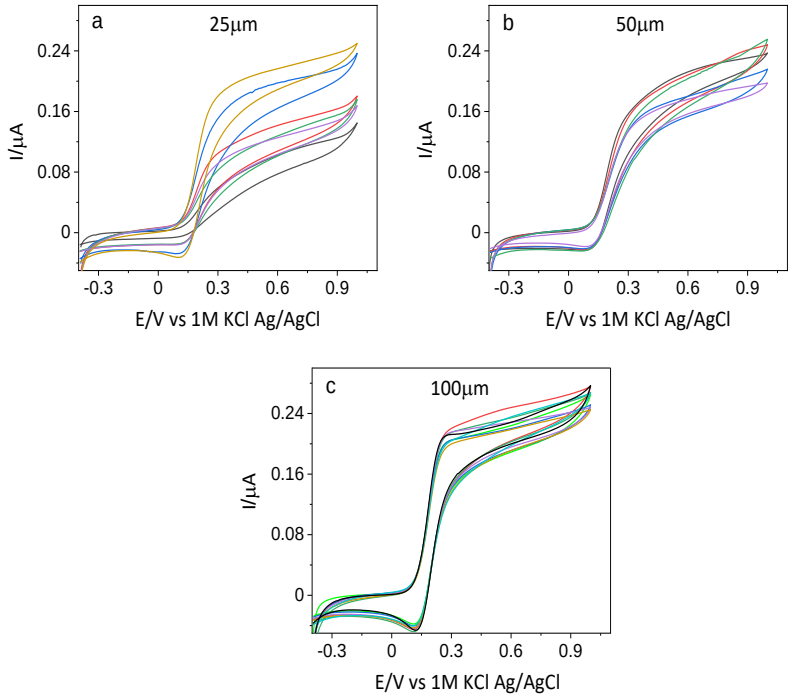

Fig.5 Cyclic voltammograms of electrodes of different sizes (a)25, (b)50 and (c)100µm width in 1 mM FcDM and 0.1 M KNO_3. Each set of electrodes comes from the same plate.

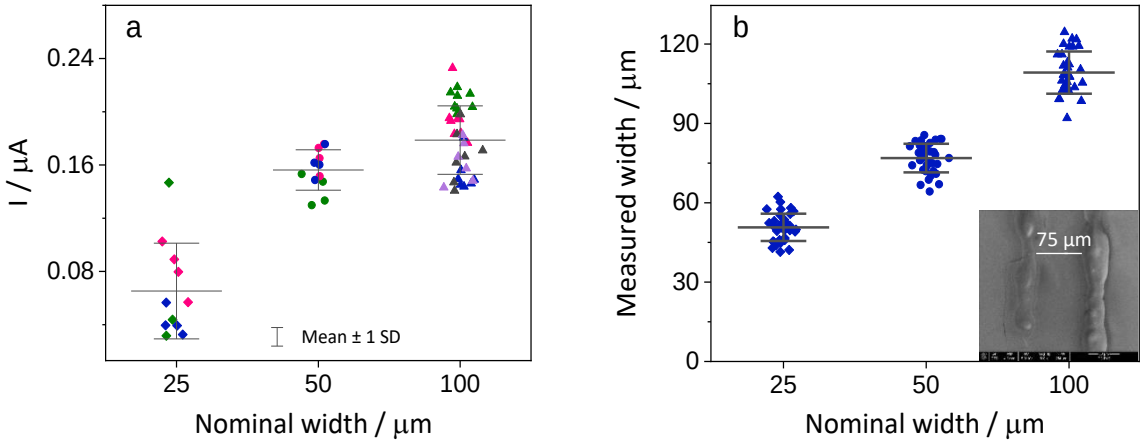

Fig.6 Reproducibility of electrode signals with respect to their nominal width are shown. a) gives the comparison of current results obtained from the cyclic voltammograms of the electrodes at 0.29V, diamond shapes represent the 25 µm, circles the 50 µm, and triangles the 100µm wide electrodes. Each colour represents a different ITO plate, b) gives the comparison of the width of the electrodes as measured by SEM technique. The diamond shapes represent 25 µm, circles the 50 µm, and triangles the 100µm wide electrodes from different plates. The inset shows an example of SEM image of an electrode with 50 µm nominal width.

Impedance spectroscopy

The stability of the system was assured by conducting potentiostatic reading at a fixed potential against open circuit potential (OCP). The first 30 minutes duration was measured with only DMEM in the well, which was then spiked with HeLa cells and their attachment on to the electrodes were observed for 60 minutes. Later, trypsin was introduced to the well in order to track the detachment separation of these cells from the electrodes and studies were continued for an additional 30 minutes. Any current or voltage input to the setup in the absence of cells with only the medium as an electrolyte is merely interfacial impedance in series with ionic solution conductivity.

As anticipated, our results showed lower resistance values and a more relaxed growth pattern during the first 30 minutes of recording compared to growth while the cells were making close contact with the electrode surface. This attachment of the cells results in a barrier that the impedance signals must cross before achieving the solution resistance. The resultant output is a combination of resistive and

capacitive elements. While the insulating cell membranes are responsible for the capacitive effects, the resistive effect is due to the ionic properties of cytoplasm[30]. Although inspection of cell responses for 30 minutes after the addition of trypsin did not completely remove them from the substrate contact, reducing the cell layer resistance to the point where the final signal resembled those throughout the absence of cells, it was evident that within this short period of time a considerable portion of the cells was successfully detached from the electrode contact.

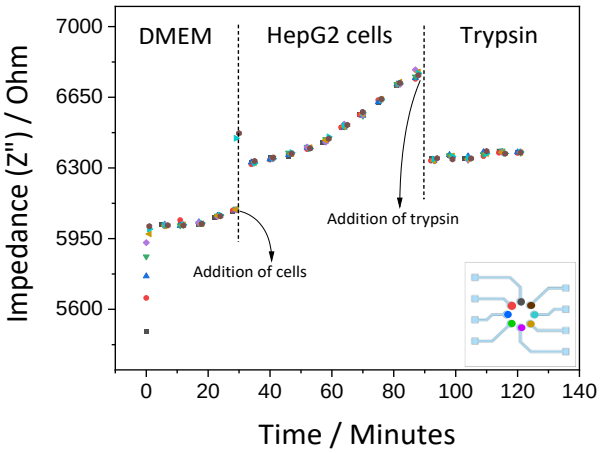

Fig. 7 Impedance spectra of HepG2 cell culture measured at 100 Hz showing cell adhesion and detachment (Short-term measurements lasting 2 hours) Each color represents a different electrode.

The responses of HepG2 cells were also studied through recording impedance alteration over time. It was noted that the resistance component Z' does not change significantly because there are still noticeable intercellular voids. HepG2 form spheroids on the surface of culture vessels rather than confluent layers as HeLa cells. What is more, with this cell population, the adherence interaction did not appear to be strong enough to give considerable change in Z'. However, when it comes to the capacitance component, Z", accountable changes can be seen within the measurement conditions. Thus, the Z" element validates to be more dependable variable for us. The figure 7 illustrates the real-time monitoring of the impedance evaluations for 2D HepG2 cell culture. Comparable signals were obtained from all 8 electrodes.

Conclusions

The objective of this work was low-cost fabrication of ITO electrodes through a novel laser assisted method. We successfully optimized the cutting of ITO coated glass plates into functional electrodes with a CO_2 laser. The electrodes of different shapes and sizes were prepared using two different methods. For the smaller rectangular shaped microelectrodes (smallest widths optimized were 25, 50 and 100 µm wide), direct patterning was used, while *in-situ* stencil fabrication followed by etching was observed as the best practice for larger circular shaped electrodes (diameter 1.75 mm, 2.41 mm^2 of geometrical surface area). All the electrodes and electrode arrays thus fabricated, demonstrated stable and reproducible signals. Cost-effective, easily fabricated, simple, and handy ITO electrodes we presented here can be treated as any contemporary working electrode in use and as a tool in several fields like sensing, bio-sensing, EWOD, microfluidics, cell culture studies and much more. As a demonstration, we used the electrode arrays for cell culture characterizations using electrochemical impedance spectroscopy (EIS).

Author Contributions

KKV – Investigation, Formal analysis, Writing – original draft; MSF – Investigation, methodology; WR – investigation; EJ – Investigation; MJN – conceptualisation, methodology, investigation, formal analysis, writing – review & editing, supervision; EWN – conceptualisation, methodology, investigation, writing – review & editing, supervision, funding acquisition.

Conflicts of interest

There are no conflicts to declare.

Acknowledgements

EWN, KKV, EJ thank The National Centre for Research and Development, Poland, for funding under grants LIDER/38/0138/L-9/17/NCBR/2018. MSF acknowledges that this publication is part of a project that has received funding from the European Union's Horizon 2020 research and innovation programme under the Marie Sklodowska-Curie grant agreement No. 847413. Scientific work published as part of an international co-financed project founded from the programme of the Minister of Science and Higher Education entitled "PMW" in the years 2020 - 2024; agreement no. 5005/H2020-MSCA-COFUND/2019/2. WR thanks Norway Grants 2014–2021 via the National Centre for Research and Development (NOR/POLNOR/UPTURN/0060/2019).

We would like to also acknowledge Ms Zuzanna Zambrowska who fabricated the first few sets of laser etched ITO electrodes.

References

[1] A. Stadler, Transparent Conducting Oxides—An Up-To-Date Overview, Materials. 5 (2012) 661–683. https://doi.org/10.3390/ma5040661.

[2] E.B. Aydın, M.K. Sezgintürk, Indium tin oxide (ITO): A promising material in biosensing technology, TrAC Trends in Analytical Chemistry. 97 (2017) 309–315. https://doi.org/10.1016/j.trac.2017.09.021.

[3] C.G. Granqvist, A. Hultåker, Transparent and conducting ITO films: New developments and applications, Thin Solid Films. 411 (2002) 1–5. https://doi.org/10.1016/S0040-6090(02)00163-3.

[4] H.B. Lee, W.Y. Jin, M.M. Ovhal, N. Kumar, J.W. Kang, Flexible transparent conducting electrodes based on metal meshes for organic optoelectronic device applications: A review, Journal of Materials Chemistry C. 7 (2019) 1087–1110. https://doi.org/10.1039/c8tc04423f.

[5] Z. Zhuang, D. Iida, P. Kirilenko, M. Velazquez-Rizo, K. Ohkawa, Optimal ITO transparent conductive layers for InGaN-based amber/red light-emitting diodes, Opt. Express. 28 (2020) 12311–12321. https://doi.org/10.1364/OE.389725.

[6] Chinky, P. Kumar, V. Sharma, P. Malik, K.K. Raina, Nano particles induced vertical alignment of liquid crystal for display devices with augmented morphological and electro-optical characteristics, Journal of Molecular Structure. 1196 (2019) 866–873. https://doi.org/10.1016/j.molstruc.2019.06.045.

[7] G. Lucarelli, T.M. Brown, Development of Highly Bendable Transparent Window Electrodes Based on MoOx, SnO2, and Au Dielectric/Metal/Dielectric Stacks: Application to Indium Tin Oxide (ITO)-Free Perovskite Solar Cells, Frontiers in Materials. 6 (2019) 1–11. https://doi.org/10.3389/fmats.2019.00310.

[8] M. Si, J. Andler, X. Lyu, C. Niu, S. Datta, R. Agrawal, P.D. Ye, Indium–Tin-Oxide Transistors with One Nanometer Thick Channel and Ferroelectric Gating, ACS Nano. 14 (2020) 11542–11547. https://doi.org/10.1021/acsnano.0c03978.

[9] J.Y. Zhou, J.L. Bai, H. Zhao, Z.Y. Yang, X.Y. Gu, B.Y. Huang, C.H. Zhao, L. Cairang, G.Z. Sun, Z.X. Zhang, X.J. Pan, E.Q. Xie, Gas sensing enhancing mechanism via doping-induced oxygen vacancies for gas sensors based on indium tin oxide nanotubes, Sensors and Actuators B: Chemical. 265 (2018) 273–284. https://doi.org/10.1016/j.snb.2018.03.008.

[10] X. Huang, W. Shi, J. Li, N. Bao, C. Yu, H. Gu, Determination of salivary uric acid by using poly(3,4-ethylenedioxythipohene) and graphene oxide in a disposable paper-based analytical device, Analytica Chimica Acta. 1103 (2020) 75–83. https://doi.org/10.1016/j.aca.2019.12.057.

[11] S. Sharma, A. Kumar, N. Singh, D. Kaur, Excellent room temperature ammonia gas sensing properties of n-MoS2/p-CuO heterojunction nanoworms, Sensors and Actuators B: Chemical. 275 (2018) 499–507. https://doi.org/10.1016/j.snb.2018.08.046.

[12] A. Celebanska, M.S. Filipiak, A. Lesniewski, E. Jubete, M. Opallo, Nanocarbon electrode prepared from oppositely charged nanoparticles and nanotubes for low-potential thiocholine oxidation, Electrochimica Acta. 176 (2015) 249–254. https://doi.org/10.1016/j.electacta.2015.06.143.

[13] D. Zhang, A. Tavakoliyaraki, Y. Wu, R.A.C.M.M. van Swaaij, M. Zeman, Influence of ITO deposition and post annealing on HIT solar cell structures, Energy Procedia. 8 (2011) 207–213. https://doi.org/10.1016/j.egypro.2011.06.125.

[14] K.A. Sierros, N.J. Morris, K. Ramji, D.R. Cairns, Stress–corrosion cracking of indium tin oxide coated polyethylene terephthalate for flexible optoelectronic devices, Thin Solid Films. 517 (2009) 2590–2595. https://doi.org/10.1016/j.tsf.2008.10.031.

[15] V.B. Nam, T.T. Giang, S. Koo, J. Rho, D. Lee, Laser digital patterning of conductive electrodes using metal oxide nanomaterials, Nano Convergence. 7 (2020). https://doi.org/10.1186/s40580-020-00232-9.

[16] J.H. Kim, K.A. Jeon, G.H. Kim, S.Y. Lee, Electrical, structural, and optical properties of ITO thin films prepared at room temperature by pulsed laser deposition, Applied Surface Science. 252 (2006) 4834–4837. https://doi.org/10.1016/j.apsusc.2005.07.134.

[17] N. Mokhtarifar, F. Goldschmidtboeing, P. Woias, ITO/Glass as Extended-Gate of FET: A Low-Cost Method for Differential pH-Sensing in Alkaline Solutions, Journal of The Electrochemical Society. 166 (2019) B896–B902. https://doi.org/10.1149/2.0401912jes.

[18] H.M. Reinhardt, P. Maier, H.C. Kim, D. Rhinow, N. Hampp, Nanostructured Transparent Conductive Electrodes for Applications in Harsh Environments Fabricated via Nanosecond Laser-Induced Periodic Surface Structures (LIPSS) in Indium–Tin Oxide Films on Glass, Advanced Materials Interfaces. 6 (2019) 1–6. https://doi.org/10.1002/admi.201900401.

[19] M. Kundys, M. Nejbauer, M. Jönsson-Niedziolka, W. Adamiak, Generation–Collection Electrochemistry Inside a Rotating Droplet, Anal. Chem. 89 (2017) 8057–8063. https://doi.org/10.1021/acs.analchem.7b01533.

[20] W. Chen, P. Ackerson, P. Molian, CO2 laser welding of galvanized steel sheets using vent holes, Materials & Design. 30 (2009) 245–251. https://doi.org/10.1016/j.matdes.2008.05.009.

[21] H.-B. Liu, H.-Q. Gong, Templateless prototyping of polydimethylsiloxane microfluidic structures using a pulsed CO 2 laser, Journal of Micromechanics and Microengineering. 19 (2009) 037002. https://doi.org/10.1088/0960-1317/19/3/037002.

[22] N.C. Speller, G.G. Morbioli, M.E. Cato, T.P. Cantrell, E.M. Leydon, B.E. Schmidt, A.M. Stockton, Cutting edge microfluidics: Xurography and a microwave, Sensors and Actuators B: Chemical. 291 (2019) 250–256. https://doi.org/10.1016/j.snb.2019.04.004.

[23] V. Radonić, S. Birgermajer, I. Podunavac, M. Djisalov, I. Gadjanski, G. Kitić, Microfluidic sensor based on composite left-right handed transmission line, Electronics (Switzerland). 8 (2019). https://doi.org/10.3390/electronics8121475.

[24] G. Chitnis, Z. Ding, C.L. Chang, C.A. Savran, B. Ziaie, Laser-treated hydrophobic paper: An inexpensive microfluidic platform, Lab on a Chip. 11 (2011) 1161–1165. https://doi.org/10.1039/c0lc00512f.
[25] M. Rashiku, S. Bhattacharya, Fabrication Techniques for Paper-Based Micro fl uidic Devices, in: Paper Microfluidics, 2019: pp. 29–45. https://doi.org/10.1007/978-981-15-0489-1_3.
[26] S. Deshmukh, P. Jakobczyk, M. Ficek, J. Ryl, D. Geng, R. Bogdanowicz, Tuning the Laser-Induced Processing of 3D Porous Graphenic Nanostructures by Boron-Doped Diamond Particles for Flexible Microsupercapacitors, Adv Funct Materials. 32 (2022) 2206097. https://doi.org/10.1002/adfm.202206097.
[27] L. Ge, Q. Hong, H. Li, C. Liu, F. Li, Direct-Laser-Writing of Metal Sulfide-Graphene Nanocomposite Photoelectrode toward Sensitive Photoelectrochemical Sensing, Advanced Functional Materials. 29 (2019) 1–10. https://doi.org/10.1002/adfm.201904000.
[28] Q. Hassan, S. Ahmadi, K. Kerman, Recent advances in monitoring cell behavior using cell-based impedance spectroscopy, Micromachines. 11 (2020). https://doi.org/10.3390/MI11060590.
[29] S. Ramasamy, D. Bennet, S. Kim, Drug and bioactive molecule screening based on a bioelectrical impedance cell culture platform, International Journal of Nanomedicine. 9 (2014) 5789–5809. https://doi.org/10.2147/IJN.S71128.
[30] A.R.A. Rahman, J. Register, G. Vuppala, S. Bhansali, Cell culture monitoring by impedance mapping using a multielectrode scanning impedance spectroscopy system (CellMap), Physiological Measurement. 29 (2008). https://doi.org/10.1088/0967-3334/29/6/S20.
[31] L. Liu, S. Yellinek, I. Valdinger, A. Donval, D. Mandler, Important Implications of the Electrochemical Reduction of ITO, Electrochimica Acta. 176 (2015) 1374–1381. https://doi.org/10.1016/j.electacta.2015.07.129.